Sensitive detection of nitric oxide using seeded parametric four-wave mixing

Mark J. Fernée, Peter F. Barker, Alan E. W. Knight, and Halina Rubinsztein-Dunlop

Citation: The Journal of Chemical Physics **108**, 6291 (1998); doi: 10.1063/1.476036
View online: http://dx.doi.org/10.1063/1.476036
View Table of Contents: http://scitation.aip.org/content/aip/journal/jcp/108/15?ver=pdfcov
Published by the AIP Publishing

Sensitive detection of nitric oxide using seeded parametric four-wave mixing

Mark J. Fernée
Molecular Dynamics Laboratory, Faculty of Science, Griffith University, Nathan, Qld., Australia, 4111

Peter F. Barker[a)]
Laser Science Centre, Physics Department, University of Queensland, St. Lucia, Qld., Australia, 4072

Alan E. W. Knight
Molecular Dynamics Laboratory, Faculty of Science, Griffith University, Nathan, Qld., Australia, 4111

Halina Rubinsztein-Dunlop
Laser Science Centre, Physics Department, University of Queensland, St. Lucia, Qld., Australia, 4072

(Received 6 November 1997; accepted 7 January 1998)

A sensitive near-resonant four-wave mixing technique based on two-photon parametric four-wave mixing has been developed. Seeded parametric four-wave mixing requires only a single laser as an additional phase matched ''seeder'' field is generated via parametric four-wave mixing of the pump beam in a high gain cell. The seeder field travels collinearly with the pump beam providing efficient nondegenerate four-wave mixing in a second medium. This simple arrangement facilitates the detection of complex molecular spectra by simply scanning the pump laser. Seeded parametric four-wave mixing is demonstrated in both a low pressure cell and an air/acetylene flame with detection of the two-photon $C\ ^2\Pi(v'=0)\leftarrow X\ ^2\Pi(v''=0)$ spectrum of nitric oxide. From the cell data a detection limit of 10^{12} molecules/cm^3 is established. A theoretical model of seeded parametric four-wave mixing is developed from existing parametric four-wave mixing theory. The addition of the seeder field significantly modifies the parametric four-wave mixing behaviour such that in the small signal regime, the signal intensity can readily be made to scale as the cube of the laser pump power while the density dependence follows a more familiar square law dependence. In general, we find excellent agreement between theory and experiment. Limitations to the process result from an ac Stark shift of the two-photon resonance in the high pressure seeder cell caused by the generation of a strong seeder field, as well as a reduction in phase matching efficiency due to the presence of certain buffer species. Various optimizations are suggested which should overcome these limitations, providing even greater detection sensitivity. © *1998 American Institute of Physics.* [S0021-9606(98)01014-9]

I. INTRODUCTION

Resonance enhanced four-wave mixing (FWM) comprises a series of nonlinear techniques which have been extensively studied for use in spectroscopy and for sensitive detection of atoms and molecules. These techniques share the advantage of generating a coherent signal beam which propagates in a direction determined by a phase matching condition. One of the simplest and most sensitive of these techniques is resonance enhanced degenerate four-wave mixing (DFWM), which has found extensive application in gas phase detection and spectroscopy of atoms and molecules.[1,2] As this technique only uses a single wavelength source, the phase matching must be satisfied geometrically with the FWM region determined by the region of beam overlap. This gives DFWM good spatial resolution. However, compared to direct absorption techniques and laser induced fluorescence (LIF), it requires complicated alignment and is somewhat susceptible to scattered light interference. Nevertheless, DFWM has shown itself to be a sensitive technique, suitable for the detection of trace species in combustion environments,[1] as has a variation of DFWM, two-color laser induced grating spectroscopy (TC-LIGS), which was introduced as a sensitive probe of higher lying excited states and congested spectra.[3] While both DFWM and TC-LIGS are FWM techniques, they can also be interpreted as coherent scattering from a laser induced volume grating which is generated in the medium.[4] This grating is defined by region of intersection of two laser beams and is used to deflect a third beam in a direction determined by the phase matching condition, which is also the Bragg condition. Therefore, the signal may result from both fully coherent processes *and* physical scattering. An example of physical scattering is that due to thermally induced refractive index gratings which result from the conversion of laser light to heat, usually through collisional quenching.[5,6]

The application of resonant FWM techniques to the detection of nitric oxide (NO) is of particular interest as NO is a major pollutant species generated in most combustion processes. The formation, detection, characterization, and quantification of NO has been thoroughly investigated using a

[a)]Present address: Department of Mechanical and Aerospace Engineering, Princeton University, Princeton, NJ.

variety of diagnostics including DFWM and TC-LIGS.[7,8] In particular, DFWM has been used for detection of NO in flames,[1] in the study of the effect of buffer gases,[6] thermal gratings[9] and line shape.[2,10,11] Most of the DFWM studies correspond to the detection of the $A\ ^2\Sigma^+ \leftarrow X\ ^2\Pi$ single photon transition which provides the greatest detection sensitivity and represents the only uv accessible single photon transition in NO. While no detection limit for NO using DFWM has been explicitly stated, the detection of 400 ppm of NO generated in a $H_2/N_2/O_2$ flame with a maximum signal to noise ratio of 2000,[1] suggests a detection limit of approximately 10 ppm. Two-photon resonant DFWM has also been used to detect the $A\ ^2\Sigma^+ \leftarrow X\ ^2\Pi$ transition in NO. This required significantly increased pump energy and tight focusing[12] resulting in a detection sensitivity some 4 orders of magnitude poorer than that obtained using single photon resonant DFWM.

Another FWM technique, parametric four-wave mixing (PFWM), is a nonlinear process analogous to parametric generation in crystals. As FWM can in general be described as a nonlinear $\chi^{(3)}$ process,[13] it is possible to observe PFWM in both liquid and gaseous media which possess inversion symmetry. Two-photon resonant PFWM typically involves nonlinear frequency conversion of two pump photons into both an ''ultraviolet'' and ''infrared'' photon via the interaction of a two-photon transition with a dipole coupled intermediate state. This technique has historically been used for vacuum ultraviolet (vuv) generation in metal vapours and noble gases.[14–16] Unlike DFWM and TC-LIGS, which are degenerate FWM schemes and can be viewed as the scattering of a probe beam from a laser induced grating, PFWM is a nondegenerate FWM process which can be made to satisfy collinear phase matching conditions, generating photons with entirely different wavelengths to those of the pump beam. In this case the direction of propagation is simply defined by the direction of the pump beam and the two signal photons may be readily detected using dispersing prisms and appropriate filters.

Theoretical models of PFWM suggest that the strong parametric fields, which couple the ground state to the upper excited state, can suppress excited state population transfer due to destructive interference with the two-photon pump process. This destructive interference was first observed with the suppression of amplified spontaneous emission in sodium due to the presence of strong parametric fields.[17,18] It has also been supported by direct LIF detection of excited state population transfer which indicated that population transfer is almost entirely suppressed when strong parametric fields are present.[19] This cancellation of population transfer is in distinct contrast to the saturation of population transfer common to DFWM[10] and TC-LIGS and other resonant absorption based techniques. Population saturation results in optical bleaching which effectively limits the signal (or degrades it in the case of laser induced grating spectroscopy). However, interference induced population cancellation requires a detailed balance be reached between the pump field and the two signal fields. Therefore, any change in the pump field results in a proportional change in both PFWM signal fields. In this two-photon cancellation regime the signal intensity becomes directly proportional to the pump field intensity. This behavior can be advantageous as it allows the use of greater pump field strengths for increased sensitivity.

PFWM has only recently been demonstrated in molecular species.[20,21] This has included the spectroscopic observation of the $C\ ^2\Pi(v=0)$ state of nitric oxide by Ishii *et al.*,[21] who present both ultraviolet and infrared PFWM signal spectra obtained using a cell with 10 Torr of NO and a strongly focused pump beam. Based on the high signal to noise ratio observed in their results, Ishii *et al.* suggested PFWM for use as a sensitive spectroscopic tool.

The primary disadvantage of PFWM is the low effective gain due to the use of weak two-photon pump transitions and the simultaneous generation of both ultraviolet and infrared fields. While the paired generation of both the ultraviolet and infrared fields from vacuum fluctuations has been shown to give rise to a novel nonclassical two-photon squeezed state,[22] it severely restricts the small signal gain of the process. The combination of weak two-photon line strength and paired generation of PFWM fields therefore restricts this process to high pressure applications where the gain can be made sufficiently large.

The introduction of an extra field to enhance nondegenerate two-photon resonant FWM efficiency has been studied theoretically by Harris *et al.*[23] and Petch *et al.*[24] as well as experimentally in atomic species by Zhang *et al.*,[25] Jain *et al.*[26] Czarnetzki and Döbele also reported significant enhancement of the FWM efficiency in molecular hydrogen by introducing an extra field into the PFWM transition.[20] While these investigations all reported significant enhancement of the FWM process, in all cases the extra field was provided by a second laser which significantly complicates the process of tuning across wide spectral ranges necessary for obtaining complex molecular spectra. As these investigations were concerned with the efficiency of nonlinear frequency conversion, tunability and experimental simplicity was not an issue of concern.

We have recently developed a new and simple means of introducing an extra field into the FWM process.[19,27,28] This is accomplished by cascading two PFWM media, such that a high density, high gain medium can be used to generate the extra seeder field for use in the second low density medium. This simple arrangement which we call seeded parametric four-wave mixing (SPFWM) provides automatic phase matching of the seeder field in the low density medium over a broad laser tuning range, facilitating the detection of complex molecular spectra. SPFWM has been demonstrated with the detection of trace amounts of NO in a cell[27] as well as the detection of nascent NO generated in a flame.[28] The sensitivity of SPFWM was also demonstrated with the detection of trace quantities of sodium in a flame, displaying an absolute sensitivity of 5×10^9 atoms/cm^3.[19]

In this paper we discuss the suitability of SPFWM for trace detection of nitric oxide and for molecular diagnostic applications. The theory is described in detail and the comparison with experiment is presented. Important issues such as phase matching and strong field effects are discussed along with the unique features of the SPFWM signal.

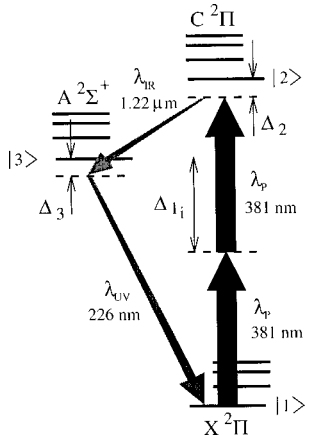

FIG. 1. The nitric oxide level scheme used for PFWM. The ground state, $X\ ^2\Pi$, the excited state, $C\ ^2\Pi$ and the intermediate state, $A\ ^2\Sigma^+$, manifolds are indicated with FWM occurring amongst the $v=0$ vibronic levels. The relevant detunings are also indicated, with the pump detuning, Δ_{1_i}, indicating a sum over the intermediate state manifold.

II. THEORY

We consider a three level ladder system with the middle level dipole coupled to both the upper and lower levels. Driving this system with a strong laser field which is nearly two-photon resonant with the ground and upper states can give rise to FWM by the simultaneous emission of two photons which, to satisfy phase matching requirements, are nearly but not exactly resonant with the two intermediate transitions. If the intermediate level lies asymmetrically between the upper and lower levels, the emitted photons will be emitted at wavelengths which are both longer and shorter than that of the pump photons (i.e., PFWM). A diagram representing the relevant transitions in NO is shown in Fig. 1, indicating the various detunings. Here, Δ_{1_j} represents the single photon detuning of the pump laser from the closest manifold of dipole coupled intermediate states. This detuning is included in the sum over intermediate states contained in the two-photon coupling term. Δ_2 represents the detuning of the pump from two-photon resonance with the upper state and Δ_3 represents the detuning of the two emitted photons from the intermediate state resonance that occurs as a result of phase matching requirements.

For SPFWM, the infrared seeder field is simply provided by the infrared component of the PFWM fields generated in a high gain medium. The seeder field propagates collinearly with the pump beam into low gain medium where it acts to stimulate the growth of the parametric fields. As the seeder field is not necessarily a strong field, it is likely to be intimately coupled to the signal field evolution in the FWM process, so established FWM theory[14] will not be appropriate for much of the field evolution. Therefore, the introduction of the seeder field into the FWM medium is best understood in terms of PFWM theory, where the initial infrared field amplitude is no longer zero, but represents some finite fraction of the pump amplitude.

The field amplitude evolution equations are obtained directly from Maxwell's equations in the slowly varying envelope approximation. In the plane wave approximation these equations are determined using

$$\frac{d\mathscr{E}_k(z)}{dz}=\frac{i\omega_k}{2\epsilon_0 n(\omega_k)c}\mathscr{P}_k(z), \tag{1}$$

where $\mathscr{E}_k(z)$ is a plane-wave Fourier component of the electric field at a frequency ω_k propagating in the z direction, $\mathscr{P}_k(z)$ is the associated Fourier component of the polarization, $n(\omega_k)$ is the refractive index of the medium and all other symbols have their usual meaning.

The medium polarization can be expanded in powers of the electric field. For gases and liquids, only odd powers are present due to inversion symmetry of the medium. To treat FWM we only require terms to third order in the electric field and so write

$$P(r,t)=\epsilon_0[\chi^{(1)}E(r,t)+\chi^{(3)}E(r,t)^3], \tag{2}$$

where $\chi^{(1)}$ and $\chi^{(3)}$ represent the linear and nonlinear susceptibilities, respectively.

When the electric field is written as a Fourier series, the different nonlinear processes can be readily identified using this notation.

The susceptibilities can be determined by considering a microscopic model of the medium. Using semiclassical quantum theory, where the medium is quantized but the fields are only considered as classical amplitudes, the field induced polarization of the medium can be determined by calculating the trace of the density matrix describing a molecular system, $\rho(t)$ with the electric dipole operator, μ,

$$P(r,t)=N\ \overline{\mathrm{Tr}(\rho(t)\mu)}, \tag{3}$$

where N is the density of molecules in the region around the point, r, and the bar over the trace represents an orientation average corresponding to an ensemble of molecules with random orientations with respect to the field. For nonlinear interactions, this average is not always easy to calculate, however, in our case it simply represents a scaling factor which can be neglected.

The calculation of the appropriate density matrix elements is accomplished by solving the density matrix equations

$$i\hbar\frac{\partial\rho(t)}{\partial t}=[H,\rho(t)], \tag{4}$$

where H is the total system Hamiltonian which, in the limit of weak interaction, can be expressed in terms of a free Hamiltonian representing the unperturbed energy levels of the system and an interaction Hamiltonian. In the electric dipole approximation, the interaction Hamiltonian, H_I represents the interaction of the electric dipole with the electric field via

$$H_I=-\mu E. \tag{5}$$

By solving the density matrix equation of motion, Eq. (4), the medium polarization and hence the equations for the evolution of the field can be determined. In general, the solution of Eq. (4) is extremely complicated. However, for

weak interactions, the density matrix equation may be solved perturbatively.[29] Solutions to third order are necessary to describe FWM.

We consider the molecular system depicted in Fig. 1 as essentially a three level system. Alternative FWM processes occurring via other intermediate states may be present but are not considered in this treatment. Any such alternative FWM process will only be coupled via the pump beam, so in the limit of minimal pump energy depletion alternative FWM processes will not be coupled and so evolve independently. While the individual FWM process may strongly couple only three levels of the available manifold of states, the other states must be considered in order to determine the appropriate phase matching condition. Using the third order perturbation solutions for the density matrix evolution and retaining only near resonant terms, the appropriate polarization components have been derived and substituted into the slowly varying envelope equation, Eq. (1), to obtain the field evolution equations. As this approach was extensively developed elsewhere,[17] we only give the results for the case of two-photon resonant pumping where $\Delta_2=0$ and perfect phase matching, $\Delta k=0$. In this case we explicitly consider the phase matching proximity to the single photon resonance where the detuning, Δ_3 is comparable to the transition linewidth, $2\Gamma_{31}$ and so we also include linear susceptibility terms for the uv signal field and pump field. For this treatment we assume that the refractive index for the 1.22 μm infrared field is close to unity and so an absorption term for the ir field can be neglected. The resultant field evolution equations are

$$\frac{d\mathscr{E}_{\rm uv}}{dz}=\frac{i\omega_{\rm uv}}{2c}\,[\,|\chi_{\rm FWM}|\mathscr{E}_{\rm ir}^{*}\mathscr{E}_P^2 e^{i(\phi_M-\beta)} - i|\chi_{\rm TPA}||\mathscr{E}_{\rm ir}|^2\mathscr{E}_{\rm uv}e^{-i2\beta}+i|\chi_{\rm abs}(\omega_{\rm uv})|\mathscr{E}_{\rm uv}e^{-i\beta}], \tag{6a}$$

$$\frac{d\mathscr{E}_{\rm ir}}{dz}=\frac{i\omega_{\rm ir}}{2c}\,[-|\chi_{\rm FWM}|\mathscr{E}_{\rm uv}^{*}\mathscr{E}_P^2 e^{i(\phi_M+\beta)} + i|\chi_{\rm TPA}||\mathscr{E}_{\rm uv}|^2\mathscr{E}_{\rm ir}], \tag{6b}$$

$$\frac{d\mathscr{E}_P}{dz}=\frac{i\omega_P}{2c}\,[2|\chi_{\rm FWM}|\mathscr{E}_{\rm uv}\mathscr{E}_{\rm ir}\mathscr{E}_P^{*}e^{-i(\phi_M+\beta)} + 2i|\chi_{2P}||\mathscr{E}_P|^2\mathscr{E}_P+i|\chi_{\rm abs}(\omega_P)|\mathscr{E}_P], \tag{6c}$$

where $\mathscr{E}_P$ is the complex field amplitude of the pump beam, $\mathscr{E}_{\rm uv}$ is the amplitude of the 226 nm signal field and $\mathscr{E}_{\rm ir}$ is the amplitude of the 1.22 μm infrared field. The different susceptibilities are defined as

$$|\chi_{\rm FWM}|=\frac{N_J}{\hbar^3\epsilon_0\Delta_3\Gamma_{21}\sqrt{\Delta_3^2+\Gamma_{31}^2}}\left|\sum_j\ \frac{\mu_{23}\mu_{31}\mu_{13_j}\mu_{3_j2}}{\Delta_{1_j}}\right|, \tag{7a}$$

$$|\chi_{\rm TPA}|=N_J\left[\frac{|\mu_{13}\mu_{32}|^2}{\hbar^3\epsilon_0\Gamma_{21}(\Delta_3^2+\Gamma_{31}^2)}\right], \tag{7b}$$

$$|\chi_{2P}|=N_J\left[\sum_j\ \frac{|\mu_{23_j}\mu_{3_j1}|^2}{\hbar^3\epsilon_0\Delta_{1_j}^2\Gamma_{21}}\right], \tag{7c}$$

$$|\chi_{\rm abs}(\omega_{\rm uv})|=N_J\left[\frac{|\mu_{13}|^2}{3\epsilon_0\hbar\sqrt{\Delta_3^2+\Gamma_{31}^2}}\right], \tag{7d}$$

$$|\chi_{\rm abs}(\omega_P)|=\frac{N_J}{3\epsilon_0\hbar}\sum_j\ \frac{|\mu_{3_j1}|^2}{\Delta_{1_j}}, \tag{7e}$$

where N_J is the molecular number density in the initial quantum state, the μ_{ij} are the dipole matrix elements connecting the levels $|i\rangle$ and $|j\rangle$ and contain the relevant Franck–Condon and Hönl–London integrals. The sums over the index j represent all the possible vibrational-rotational levels in the $A\ ^2\Sigma^+$ state manifold that contribute to the two-photon absorption cross-section of the pump beam. The quantities $2\Gamma_{21}$ and $2\Gamma_{31}$ represent the two-photon and single photon transition linewidths which are included phenomenologically in this semiclassical treatment and we have made the approximation, $\Gamma_{23}\approx\Gamma_{31}$ in order to simplify $|\chi_{\rm TPA}|$. In Eqs. (6), the phases ϕ_M and β are defined by

$$\tan\,\phi_M=\frac{\text{Im}\ \Sigma_j(\mu_{23}\mu_{31}\mu_{13_j}\mu_{3_j2}/\Delta_{1_j})}{\text{Re}\ \Sigma_j(\mu_{23}\mu_{31}\mu_{13_j}\mu_{3_j2}/\Delta_{1_j})}, \tag{8a}$$

$$\tan\,\beta=\frac{\Delta_3}{\Gamma_{31}}. \tag{8b}$$

To proceed further we consider the approximation that FWM does not deplete the pump, so we can neglect Eq. (6c). The field equations (6) can then be expanded into their real and imaginary parts by writing the complex field amplitudes in terms of real amplitudes and phases via, $\mathscr{E}_x=A_xe^{i\phi_x}$. Therefore, we may rewrite Eqs. (6) as follows:

$$\frac{dA_{\rm uv}}{dz}=\frac{\omega_{\rm uv}}{2c}\,[-|\chi_{\rm FWM}|A_{\rm ir}A_P^2\,\sin(\Theta-\beta) + |\chi_{\rm TPA}|A_{\rm ir}^2A_{\rm uv}\cos 2\beta-|\chi_{\rm abs}(\omega_{\rm uv})|A_{\rm uv}\cos\,\beta], \tag{9a}$$

$$\frac{dA_{\rm ir}}{dz}=\frac{\omega_{\rm ir}}{2c}\,[|\chi_{\rm FWM}|A_{\rm uv}A_P^2\,\sin(\Theta+\beta)-|\chi_{\rm TPA}|A_{\rm uv}^2A_{\rm ir}], \tag{9b}$$

$$\frac{d\Theta}{dz}=-\frac{|\chi_{\rm FWM}|A_P^2}{2c}\left[\frac{\omega_{\rm uv}A_{\rm ir}}{A_{\rm uv}}\cos(\Theta-\beta)-\frac{\omega_{\rm ir}A_{\rm uv}}{A_{\rm ir}}\cos(\Theta+\beta)\right]+\frac{\omega_{\rm uv}}{2c}\,[|\chi_{\rm TPA}|A_{\rm ir}^2\sin 2\beta], \tag{9c}$$

where the new phase, Θ represents a sum of individual phases defined as follows:

$$\Theta=2\phi_P+\phi_M-\phi_{\rm uv}-\phi_{\rm ir}, \tag{10}$$

and the phase matching relationship

$$2\ \text{Re}\ \chi_{\rm abs}(\omega_P)=\text{Re}\ \chi_{\rm abs}(\omega_{\rm uv}), \tag{11}$$

which is satisfied when $\Delta k=0$, has been used to simplify the phase equation. In general, the phase matching relationship given by Eq. (11) must also include a contribution due to the dispersion of the 1.22 μm infrared field, but here we con-

sider the medium to be completely transparent at this wavelength. This may not remain true in the presence of other molecular species.

A. Simplified limiting behavior of SPFWM

If we consider phase matching to occur sufficiently far from the resonance such that the angle β approaches $\pi/2$, then the Eqs. (9) may be readily simplified as follows:

$$\frac{dA_{\mathrm{uv}}}{dz}=\frac{\omega_{\mathrm{uv}}}{2c}\left[|\chi_{\mathrm{FWM}}|A_{\mathrm{ir}}A_P^2-|\chi_{\mathrm{TPA}}|A_{\mathrm{ir}}^2A_{\mathrm{uv}}\right], \tag{12a}$$

$$\frac{dA_{\mathrm{ir}}}{dz}=\frac{\omega_{\mathrm{ir}}}{2c}\left[|\chi_{\mathrm{FWM}}|A_{\mathrm{uv}}A_P^2-|\chi_{\mathrm{TPA}}|A_{\mathrm{uv}}^2A_{\mathrm{ir}}\right]. \tag{12b}$$

These coupled equations can be decoupled and solved using the following constant of the motion:

$$\frac{A_{\mathrm{ir}}^2}{\omega_{\mathrm{ir}}}-\frac{A_{\mathrm{uv}}^2}{\omega_{\mathrm{uv}}}=\mathrm{Const}, \tag{13}$$

which results from production of photons in pairs, the constant corresponding to the difference in photon number between the two parametric fields.

We wish to consider the case corresponding to the standard PFWM, where both the uv and ir signal fields evolve from the vacuum and the case corresponding to SPFWM, where a strong ir field is present initially. At first we only consider the small signal solutions in a low density medium. For the case of both fields starting from the vacuum, the constant of the motion must be zero, whereas when a strong ir field is initially present and only the uv signal field must start from the vacuum, the constant is simply given by $n(\omega_{\mathrm{ir}})A_{\mathrm{ir}}^2(0)/\omega_{\mathrm{ir}}$, where $A_{\mathrm{ir}}(0)$ is the initial amplitude of the ir field. For Const$=0$ we find

$$A_{\mathrm{uv}}(z)\approx A_{\mathrm{uv}}(0)\exp(\alpha\sqrt{(\omega_{\mathrm{uv}}\omega_{\mathrm{ir}})}\,A_P^2z), \tag{14}$$

where $\alpha=|\chi_{\mathrm{FWM}}|/c$. While this solution exhibits exponential gain in the small signal regime, it is nonetheless governed by the initial amplitude of the signal field which is vanishingly small. Therefore, a substantial gain length is required for the signal field to grow to a significant value. This gain length is inversely proportional to both the pump intensity and the density of the medium, such that by using a high density medium and high pump intensities a reasonable gain length can be achieved. However, high number densities are contrary to our requirement and high pump intensities can cause many other problems such as ionization depletion of the ground state, strong ac Stark shifts and higher order wave mixing.

In order to significantly increase the gain of the process for use with low number densities we supply a strong initial ir ''seeder'' field. In this case the small signal response may be approximated as

$$A_{\mathrm{uv}}(z)\approx\frac{\omega_{\mathrm{uv}}}{c}\,|\chi_{\mathrm{FWM}}|A_{\mathrm{ir}}(0)A_P^2z. \tag{15}$$

Here we find that the initial behavior of the seeded system is independent of the amplitude of the initial uv field. We immediately see that the signal intensity will be proportional to the square of the number density, N_J, rather than the exponential dependence as in the unseeded case. The SPFWM signal amplitude is also proportional to the square of the pump amplitude and directly proportional to the ir seeder amplitude.

As the high density seeder medium which generates the ir seeder field operates with the same PFWM transition as the low density medium, its behavior is also governed by the coupled amplitude equations (12). However, by using a high molecular density, the gain can be made sufficiently large such that the seeder operates in the two-photon cancellation regime where the nonlinear absorption balances the parametric generation.[17]

That is,

$$A_P^2-\frac{|\chi_{\mathrm{TPA}}|}{|\chi_{\mathrm{FWM}}|}A_{\mathrm{uv}}A_{\mathrm{ir}}=0. \tag{16}$$

When this condition is satisfied and using the fact that the two parametric fields must be proportional to each other due to the paired photon generation, we find that both the uv and ir fields become linearly proportional to the pump field (if we can ignore absorption of the uv field). Therefore, if the high pressure seeder medium is operated in this two-photon cancellation regime, the seeder field will evolve in direct proportion to the pump field so that according to Eq. (15) the SPFWM signal field will scale as the cube of the pump field.

B. Numerical simulations of the SPFWM signal evolution

The coupled equations (9) may easily be solved numerically and the solutions compared in order to gain some insight into the behavior of SPFWM over a variety of operating conditions. We first compare solutions for the field evolution corresponding to different initial seeder field amplitudes, including the case of negligible initial amplitude which corresponds to the PFWM solution. These solutions are obtained at a phase matching point far away from the central resonance (i.e., $\Delta_3/\Gamma_{31}=6.3$ was used). The various susceptibilities have been chosen in order to represent the conditions in our experiment. If we ignore direct absorption of the uv signal field, we would expect the uv signal field maximum to decrease with increasing seeder intensity so that the balance defined in Eq. (16) is maintained. This expectation is still borne out in Fig. 2 along with a small but steady decrease in uv signal due to direct absorption. We also see that the seeded solutions grow rapidly from the noise until the two-photon cancellation regime is reached at which point the field starts to decrease due to direct absorption. The effect of increasing the seeder field amplitude causes a reduction in the maximum of the uv signal field when the two photon cancellation regime is reached. The extra gain length required for PFWM when both fields start with negligible amplitudes is shown here. We have used initial field amplitude ratios of $A_{\mathrm{ir}}/A_P=A_{\mathrm{uv}}/A_P=10^{-12}$ in this curve. When the ratios were reduced to 10^{-15}, the gain length required for significant uv signal growth was now longer than the length of the displayed axis. This suggests that an increase in uv

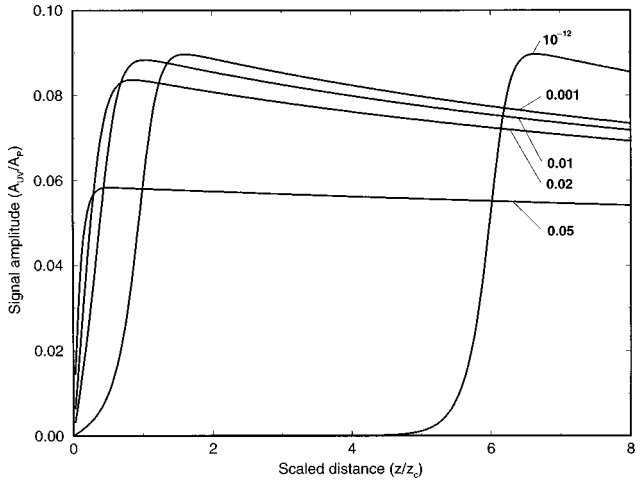

FIG. 2. Numerical simulations of SPFWM uv signal field evolution using Eq. (9), for the case of phase matching far from the resonance (i.e., $\Delta_3/\Gamma_{31}=6.3$). Solutions representing different initial seeder field amplitudes, $A_{\rm ir}/A_P$ are presented. The distance, z, is scaled using a characteristic length, $z_c=(N_J|\chi_{\rm FWM}|A_P^2\sqrt{\Delta_3^2+\Gamma_{31}^2})^{-1}$.

signal gain of many orders of magnitude may be achieved when using a strong seeder field, and forms the basis for our experimental study.

The Eqs. (9) represent SPFWM field evolution as a function of the phase matching proximity to the single photon resonance, Δ_3. This is useful in our case as we are dealing with SPFWM in a molecule which has a complex spectrum and so the SPFWM intermediate resonance will depend on the two-photon resonance that is being excited by the pump. Such complex molecular phase matching has been carefully treated by Czarnetzki and Döbele[20] whose calculations indicate that the phase matching proximity to the central resonance can vary quite markedly. Therefore, we show the effect of varying the phase matching point in Fig. 3. It is interesting to find the maximum field amplitude decreasing as Δ_3 decreases, however we also see that the gain, represented by the initial slope of each curve, increases significantly with closing proximity to the resonance. For trace species detection, high gain is most important. Therefore, we expect that the balance between proximity to the resonance and direct absorption of the signal is most important for determining good phase matching. The oscillatory behavior that becomes evident for small detuning, Δ_3, results from the changing phase of the two-photon absorption term for the uv signal field, such that the solution transitions from being over-damped to under-damped. In this near-resonance regime the true signal behavior requires the inclusion of the laser bandwidth which is beyond the scope of our theory. However, the essential features of reduced steady state signal level and increased gain should remain valid.

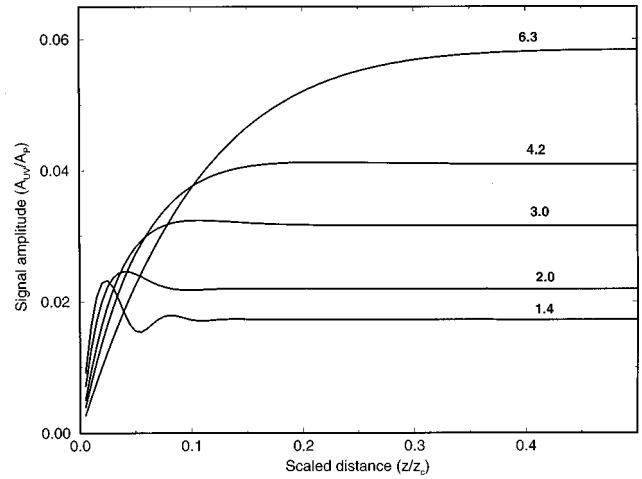

FIG. 3. Numerical simulations of SPFWM uv signal field generation using Eq. (9) for the case of seeding with an initial amplitude of $A_{\rm ir}/A_P=0.05$. Solutions representing different phase matched detunings from the intermediate resonance, Δ_3/Γ_{31}, are presented. The distance, z, is scaled using a characteristic length, $z_c=(N_J|\chi_{\rm FWM}|A_P^2\sqrt{\Delta_3^2+\Gamma_{31}^2})^{-1}$.

In the present treatment of SPFWM we have ignored certain terms that would otherwise be present in the coupled amplitude equations, such as ac Stark shift effects, multiphoton ionisation and other higher order terms. Although these various effects have been observed, the theory as presented is nevertheless consistent with the general behavior which we report in this paper.

C. Phase matching in SPFWM

The graphs of Figs. 2 and 3 are plotted on a scaled axis z/z_c where the quantity z_c represents a characteristic length within the medium and is defined by,

$$z_c=(N_J|\chi_{\rm FWM}|A_P^2\sqrt{\Delta_3^2+\Gamma_{31}^2})^{-1}. \tag{17}$$

From these graphs we see that the PFWM solution in Fig. 2 requires many characteristic lengths to build to an appreciable signal, whereas we find in the SPFWM signals can attain their maximums over distances much shorter than one characteristic length. This has important implications for phase matching in both PFWM and SPFWM.

If we include a phase mismatch term in the FWM phase via $\Theta'=\Theta+\overline{\Delta k}\,\overline{z}$, where the phase mismatch is written using the scaled quantities $\overline{\Delta k}=\Delta k z_c$ and $\overline{z}=z/z_c$, then the total field evolution described in Eq. (9) will not be significantly modified if either the gain length or the phase mismatch is sufficiently small such that the product is much smaller than unity. For PFWM, where the gain length must be large in order to produce a significant signal, only very small phase mismatches can be tolerated. However, for SPFWM only short gain lengths are required to produce a significant signal. For a gain length, $z/z_c=0.1$, a phase mismatch of the order of, $\Delta k\approx 1/z_c$ may be tolerated, which can be more than 100 times greater than the phase mismatch tolerance of PFWM under the same operating conditions.

The high phase mismatch tolerance of SPFWM is important for sensitive detection in differing environments where refractive index variations may significantly alter the phase matching conditions within the SPFWM medium relative to the PFWM medium.

III. THE EXPERIMENT

The experimental set-up is shown in Fig. 4. The pump beam is provided by a Nd:YAG (Continuum NY81) pumped dye laser (Lambda Physik Scanmate II) operating with an

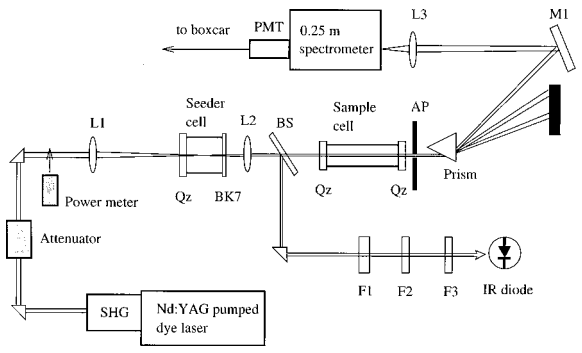

FIG. 4. The SPFWM experimental arrangement showing the high pressure seeder cell, C1 and low pressure sample cell, C2. The filter, F, consisted of a BK7 glass exit window in the seeder cell. A 200 mm focusing lens, L1 and 100 mm recollimating lens, L2 were used, with L2 positioned to produce a loose focus within the cell, C2. The prism, P, was used to separate the signal from the pump and seeder beams.

Exciton LDS 751 dye at around 763 nm. The dye laser output is then doubled, producing 10 ns pulses of up to 3 mJ at around 381 nm with a linewidth of approximately 0.2 cm^{-1}. No attempt was made to improve the beam characteristics, so we operated with a highly non-uniform beam profile. The beam can be passed through a high power symmetric wedge variable attenuator (Newport) and the power measured with a power meter (Ophir). Efforts were made to ensure the power meter could be repeatedly placed into the beam so that it provided reproducible results. The beam then passes into a focusing and recollimating section consisting of a 200 nm planoconvex quartz lens, L1, and a 100 mm biconvex quartz lens, L2 with the initial focusing lens, L1, providing a maximum pump intensity in the focal region of approximately 5×10^8 W/cm^2. This section contains the seeder cell which is 5 cm long with a quartz window on one side and a BK7 glass window on the other. When acting as a seeder cell, the BK7 element is positioned so as to totally absorb the 226 nm uv signal field. Otherwise, the quartz window could be used as the exit window such that it would transmit all the fields. The BK7 element was more than sufficient to transmit the 381 nm uv pump beam without appreciable absorption.

The recollimating lens, L2, was adjusted to obtain an appropriate gain length and gain area in the sample cell. For most of the experiment it was positioned at 365 mm from the focusing lens, L1, providing a maximum pump intensity in the focal region of the sample medium of approximately 5×10^7 W/cm^2. The lens combination, L1 and L2, were chosen such that they operated in an inverse telescope mode in order to reduce the beam area as well as provide a weak focus in the sample cell. In this way both the gain length and area were maximised in the sample cell.

A quartz plate, BS, was used to split off a few percent of the beam in order to monitor the ir seeder field. The 381 nm portion of this field was attenuated with a combination of a 355 nm dielectric mirror and an ir low pass filter (Oriel), F1, and F2, respectively, while a Schott glass filter (UG5), F3, was used to attenuate the infrared signal which was then detected with an InGaAs communications photodiode (Fujitsu).

The sample cell was typically a 10 cm glass cell with quartz windows. The light exiting the sample cell was apertured, to reduce the scattered component, and passed through a dispersing element consisting of a simple right angle prism. A beam block absorbed most of the pump radiation while the uv signal beam was reflected by a 220–240 nm dielectric mirror, M1, and coupled into a 0.25 m monochromator (GCA/McPherson) via a 100 mm quartz lens, L3. The monochromator was set at 226 nm and the exiting radiation detected with a solar blind photomultiplier tube (Hammamatsu R759). The signals from the photodiode and photomultiplier were input into a digital oscilloscope (Hewlett Packard 54510A) and boxcar averagers (SRS SR250), the output of which was digitised and the data collected and displayed on a microcomputer.

The NO was obtained as a pure gas which we further purified using a single freeze/thaw cycle such that there was no discernible discoloration in our 1 ℓ glass storage bulb. The vacuum system consisted of a single rotary vacuum pump connected to a network of copper pipe with Swagelok connections. The pressure was monitored close to the cell with a pirani/capacitance manometer dual vacuum gauge (Varian). This system provided the limiting constraint on our operating conditions. Nevertheless, our system was sufficient to give highly reproducible results which we report here.

SPFWM was also conducted in an air/acetylene flame using a slot burner with a 10 cm slot (Varian AA6), in place of the sample cell in Fig. 3. For the experiment, the flame was operated fuel rich with an equivalence ratio, $\phi=2.5$. The beams were passed approximately 20 mm above the burner head traveling parallel to the flame slot. Operation with the beams passing perpendicular to the flame slot was also conducted.

The two-photon $C\ ^2\Pi(v'=0)\leftarrow X\ ^2\Pi(v''=0)$ transition in nitric oxide was also monitored by focusing the pump beam into a 20 cm optogalvanic cell, enabling the $2+1$ resonance enhanced multi-photon ionisation (REMPI) spectrum to be recorded. The pump energy was simultaneously monitored with a photodiode in order to provide a normalization curve for the REMPI spectrum.

IV. RESULTS AND DISCUSSION

A. Low pressure cell data

In Fig. 5 we present four scans of the two-photon $C\ ^2\Pi(v'=0)\leftarrow X\ ^2\Pi(v''=0)$ spectrum of NO, obtained using various different techniques. The upper most spectrum, labeled REMPI, is the two-photon resonance enhanced ionization spectrum which we provide as a reference. The second spectrum, labeled ir seeder, is the 1.22 μm PFWM infrared seeder signal which is used to generate the SPFWM signal. The third spectrum, labeled uv signal, is the resultant SPFWM signal. The fourth spectrum, labeled uv PFWM, results from the direct detection of the 226 nm PFWM signal obtained from a low gain intermediate pressure cell and is provided for comparison with the SPFWM result.

The REMPI spectrum in Fig. 5 provides a reference two-photon $C\ ^2\Pi(v'=0)\leftarrow X\ ^2\Pi(v''=0)$ spectrum at the same 0.2 cm^{-1} resolution used for the ensuing PFWM and

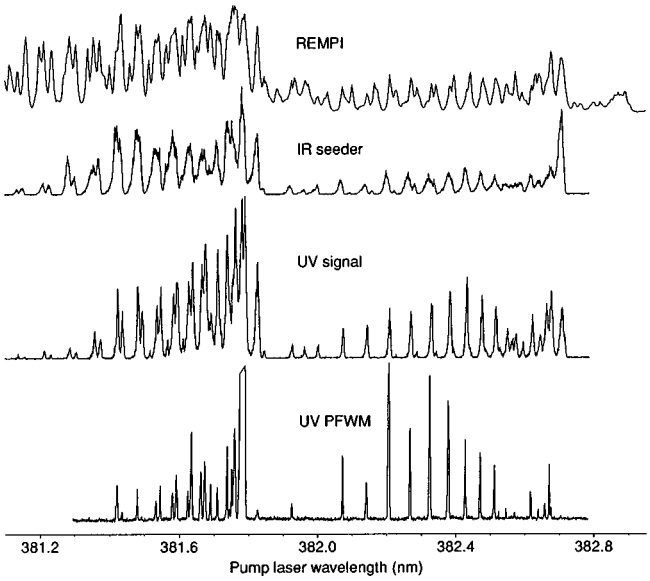

FIG. 5. A comparison of spectra representing the $C\ ^2\Pi(v'=0) \leftarrow X\ ^2\Pi(v''=0)$ transition in NO. The upper trace labeled REMPI is the two-photon resonance enhanced ionisation spectrum obtained from a cell containing 10 mbar of NO. The spectrum labeled ir seeder represents the 1.22 μm seeder field obtained with a pressure of 400 mbar of NO. The spectrum labeled uv signal was recorded simultaneously with the ir seeder spectrum and represents the 226 nm SPFWM signal obtained from 1 μbar of NO buffered with Ar to 10 mbar. The lowest trace labeled uv PFWM represents 226 nm PFWM signal obtained from a cell containing 48 mbar of NO. The intensity axis is independently scaled for each spectrum.

SPFWM experiments. The spectrum has been scaled inversely proportional to the cube of the pump pulse energy over the range of the scan and is in good agreement with the high pressure LIF spectrum obtained by Freedman[30] and the REMPI spectrum obtained by Hayden and Diebold.[31]

The ir seeder spectrum in Fig. 5 represents the 1.22 μm infrared field obtained from the high gain seeder cell which contains 400 mbar of NO. This field is then used to seed the FWM process in the low pressure cell. The resultant SPFWM uv signal obtained from the low pressure cell, containing a partial pressure of 1 μbar of NO buffered to 10 mbar with argon, is shown below the ir seeder signal for comparison. These two spectra were taken simultaneously using the experimental arrangement depicted in Fig. 4. The ir spectrum represents operation at or close to the two-photon cancellation regime which limits the ir field generation, representing a form of saturation, while the wings of each spectral feature are significantly broadened due to the extra gain at the high pressure. Thus the seeder cell provides the extra seeder field over a broad pump tuning range. However, the SPFWM signal is produced only when the pump beam is near a two-photon resonance. So the seeder field considerably enhances the FWM gain only close to the two-photon resonance and has no noticeable effect otherwise. Comparison of the SPFWM uv signal spectrum with the REMPI spectrum reveals that certain features are absent in the SPFWM uv signal spectrum, indicating that additional FWM selection rules must apply. However, proper interpretation of the SPFWM spectrum requires the development of a full spectral model including all possible FWM pathways and is beyond the scope of this paper.

The line shape asymmetry, which is observed in the SPFWM uv signal spectrum is a characteristic feature of two-photon PFWM, resulting in this case from the contribution of the $A\ ^2\Sigma^+$ state to the refractive index at the pump laser frequency. As significant FWM gain exists over a wide pump detuning range, Δ_2, the variation in refractive index with pump detuning acts to increase the gain (by moving the phase matching point closer to the intermediate state resonance, thus reducing the detuning, Δ_3) when tuning in one direction and conversely decrease the gain when tuning in the opposite direction. Thus there exists a gain asymmetry which depends on the sign of the pump laser detuning from the two-photon resonance.

The uv PFWM spectrum, which is also shown in Fig. 5, was obtained from a 10 cm cell containing 48 mbar of NO with a 100 mm focal length lens used to focus the pump beam into the cell. This spectrum shows a strong $T_Z \leftarrow X\ ^2\Pi_{1/2}$ bandhead feature,[30] which is saturated and has been purposely truncated in order to reveal the remaining spectral features in sufficient detail. This property was evident in all our pure PFWM data obtained well below the two-photon cancellation regime and indicates the exponential relationship that the signal has with the various transition strengths. At higher pressures this feature disappeared as most of the transitions are driven towards the two-photon cancellation regime. The noticeable paucity of spectral features results from the exponential dependence of the signal on both the FWM susceptibility and rotational state density [cf. Eq. (14)]. This exponential gain is also responsible for the narrow spectral features which are observed. Many of the spectral features observable in the SPFWM spectrum are absent in the PFWM spectrum due to lack of gain. Thus even in the congested bandhead regions, only a few individual lines are present. In comparison with the ir seeder spectrum, it is clear that the increase in gain due to increased molecular density eventually reveals the missing spectral features. With optimisations, we were able to obtain good quality PFWM spectra at pressures down to 5 mbar, but could find no detectable signal at 2 mbar. This strong exponential dependence on density precludes PFWM from use as a sensitive probe for molecular species.

In Fig. 6 we show a graph of the dependence of the SPFWM signal on NO partial pressure. We find that the square law scaling of the molecular density predicted by the small signal theory of Eq. (15) is clearly followed. Having established the expected small signal behavior, we can use this to determine a detection limit for NO using SPFWM, corresponding to a signal to noise ratio of 1. From inspection of the SPFWM spectrum in Fig. 5 we estimate a maximum signal to noise ratio of 100 from which we extrapolate the detection limit as 0.1 μbar or 10^{12} molecules/cm^3. This must be a conservative limit given that the largest signal is most certainly no longer following small signal behavior. This sensitivity corresponds to that required for trace species detection,[1] clearly establishing SPFWM as a sensitive laser diagnostic method.

The behavior of the SPFWM signal with changing pump

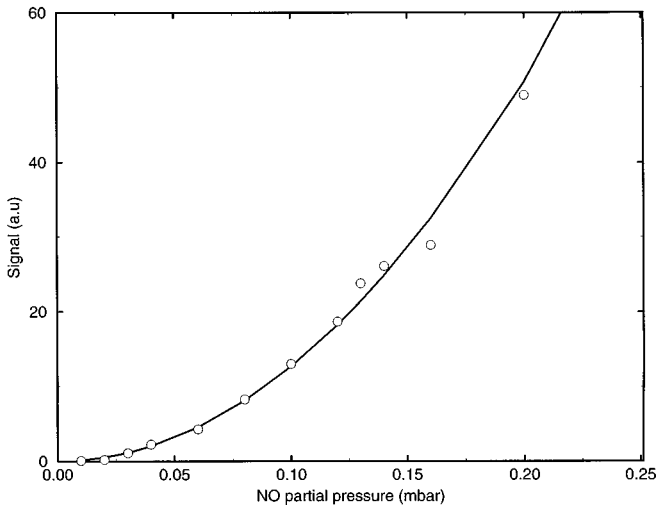

FIG. 6. The dependence of the 226 nm signal field with NO partial pressure (circles) indicating square law behavior in the small signal regime (solid line). The data were obtained from the relatively isolated $T_Z \leftarrow X\ ^2\Pi_{3/2}Q(10.5)$ transition near 382.3 nm (Ref. 30), using a 300 mbar seeder cell and buffering the sample to 100 mbar with argon.

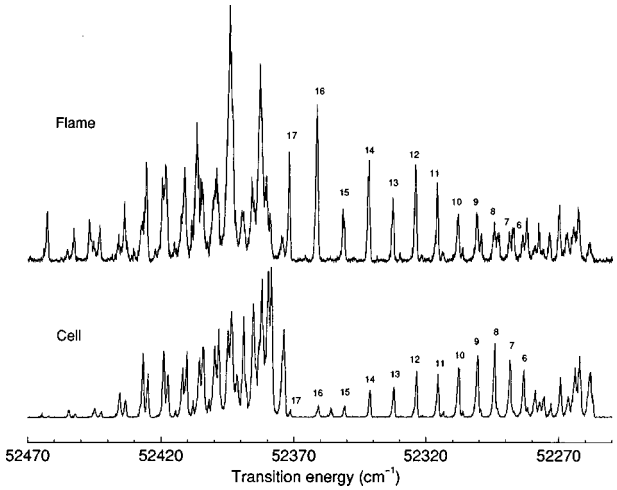

FIG. 8. A comparison of SPFWM spectra; one obtained in an air–acetylene flame with an estimated NO molecular fraction of 100 ppm (top) and the other obtained in a cell containing 1 μbar of NO buffered to 10 mbar in argon (bottom). Both spectra were obtained using 400 mbar of NO in the seeder cell and the same experimental set-up shown in Fig. 4. A series of rotational states have been labeled $(J-1/2=6\cdots17)$ for the $T_Z \leftarrow X\ ^2\Pi_{3/2}Q(J)$ transition to aid comparison of the spectra.

pulse energy is shown in Fig. 7. In the upper graph, (a), we show the SPFWM data along with a curve generated using Eqs. (6). Here we observe that the uv signal evolves past the small signal regime. We also found that a small linear absorption term had to be included in order to obtain a suitable fit in the large signal regime. The lower graph, (b), displays the corresponding behavior of the infrared seeder signal with changing pump pulse energy. The data are easily fit to a straight line, indicating that PFWM in the high pressure seeder cell is operating in the two-photon cancellation regime. This enables the SPFWM process to be modeled using Eqs. (6) where the ratio of the initial seeder field amplitude to the pump field amplitude is simply represented by a constant over the entire range of pump pulse energies.

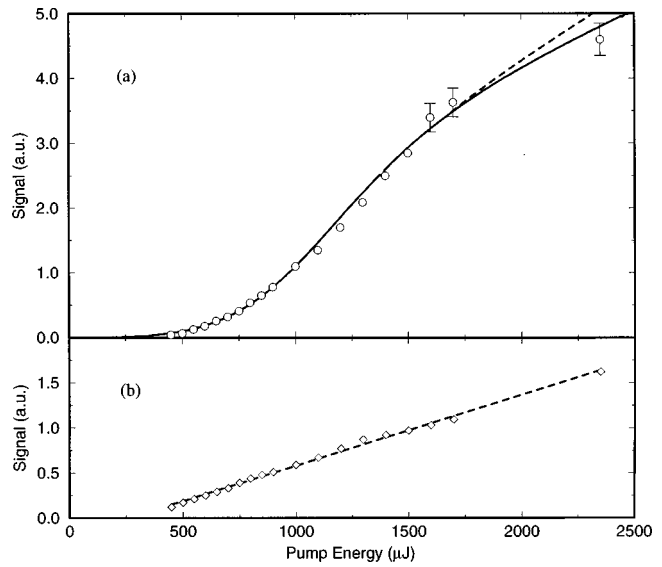

FIG. 7. The pulse energy dependence of (a), the 226 nm signal obtained from 20 μbar of NO buffered to 10 mbar with Ar, and (b), the 1.22 μm seeder signal obtained from 400 mbar of NO. A straight line is fit to the seeder data, while a curve generated by numerically integrating Eqs. (6) has been fit to the signal data. The dashed curve in (a) corresponds to the best fit obtained without the direct absorption term in Eq. (6a). The data were obtained from the $T_Z \leftarrow X\ ^2\Pi_{3/2}Q(10.5)$ transition.

Due to the high SPFWM gain, enabling a weaker focus to be employed in the signal cell, we found that we were able to generate a significantly stronger 226 nm signal field than was possible using pure PFWM in a high pressure cell. This was demonstrated by the generation of a uv signal with enough energy to cause visible fluorescence from a white card, using a signal cell with 30 mbar of NO. We found no condition, using PFWM alone, where we could generate enough uv signal to cause visible fluorescence.

B. Flame results

Having clearly established the sensitivity of SPFWM, we next applied it to the more useful and demanding task of detection of nascent concentrations of NO in a flame. An air–acetylene flame was operated fuel rich which is the usual state used in atomic absorption spectroscopy and corresponded to the most stable flame condition. For our operating fuel/air equivalence ratio of 2.5, we estimate a maximum NO concentration of 100 ppm, based on flame equilibrium calculations which predict an NO concentration of less than 20 ppm[32] with the assumption that entrained air will also add extra thermally generated NO. While this flame state represents a stoichiometry very different from that used in much of the DFWM studies of NO, the low NO concentration provides an excellent benchmark for SPFWM.

A comparison between SPFWM spectra in a cell and that obtained from the flame is shown in Fig. 8. For clarity, the values $J-1/2$ are included on various transitions of the $T_z \leftarrow X\ ^2\Pi_{(3/2)}\ Q$ branch. Here we see strong evidence of rotational energy redistribution of the ground state towards higher lying rotational states in the hot flame when compared

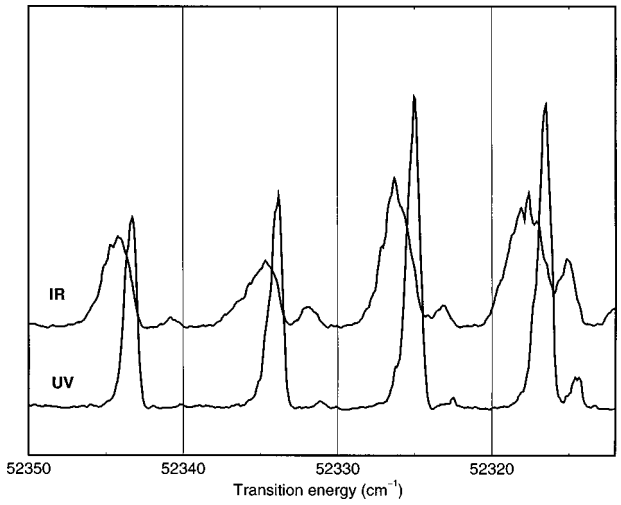

FIG. 9. A high resolution comparison of a section of the ir seeder spectrum (top) and uv SPFWM spectrum (bottom) shown in Fig. 5, indicating a shift in the ir seeder spectral features relative to those of uv SPFWM spectrum. A five point running average has been used to smooth the data.

to the room temperature cell. However, the lack of a spectral model for SPFWM precludes making a quantitative estimate of the flame temperature. Based on a signal to noise ratio of 100 and a NO concentration of 100 ppm, we estimate a detection sensitivity in the flame of 10 ppm which is comparable to that obtained using DFWM.[1]

C. The effect ac Stark shifts on SPFWM

On close examination of both the uv signal spectrum and ir seeder spectrum in Fig. 5 we find a shift of approximately 1 cm^{-1} in the spectral features of the ir seeder. In Fig. 9 we show a magnified comparison of the two spectra in a relatively isolated spectral region, which indicates the magnitude of the shift. We also find an identical shift when detecting NO generated in the air–acetylene flame using the same 400 mbar seeder arrangement, which suggests the shift is in the seeder spectrum. We believe this to be an ac Stark shift induced in the seeder cell due to the high field strengths in the tight focal region. The exact cause of the shift is not certain from this data, however, other experiments with PFWM in sodium have indicated that the shift is caused by the generated parametric fields[19] and not the pump beam. If the infrared seeder field is responsible for the observed shift we would expect the magnitude of the shifts to be correlated to the maximum of the infrared signal. This is exactly what we do see in Fig. 9 when we compare the shifts of the four strong peaks. Importantly the observed shifts are significant enough to limit the on-resonance seeder field strength in the SPFWM medium, effectively limiting the SPFWM gain.

The choice of seeder pressure and pump focusing will play an important role in further increasing the sensitivity of SPFWM. At higher cell pressures a weaker focus should result in a stronger seeder field by reducing the ac Stark shift. A change in seeder cell pressure from 300 to 400 mbar of NO has shown at least an order of magnitude increase in the detection sensitivity and suggests that further increases should be possible.

D. Influence of foreign species on phase matching

As PFWM and SPFWM are nondegenerate FWM processes, the appropriate phase matching for collinear propagation of the ir and uv signals requires that the relationship Eq. (11) be satisfied. The gain of the PFWM process depends strongly on obtaining a good balance between the pump and signal susceptibilities so that phase matching occurs sufficiently close to the central resonance. In a cell this can be accomplished by modifying the medium refractive index with the addition of a suitable buffer gas.[20,14] For NO we have found that the various PFWM transitions have significant gain and as such are suitable for generating a strong seeder field. However, if the low density SPFWM medium represents a different environment to that of the seeder cell, then the phase matching condition in the SPFWM environment can be significantly altered with respect to that of the high pressure seeder cell due to the presence of different atomic and molecular species. In this case, we would not expect the SPFWM process to be automatically phase matched.

The effect of buffer gases on PFWM efficiency was briefly studied. Argon, nitrogen, and carbon monoxide were mixed in varying proportions with NO in a 10 cm sample cell. We found that argon had a minimal effect on the PFWM signal while nitrogen and carbon monoxide both reduced the PFWM signal, the latter significantly so. This is due to the effect of the buffer gas on the refractive index of the medium, where the change in the refractive index moves the phase matching point away from the resonance, thus reducing the gain. These buffer gas results suggest that phase matching should be significantly altered in an air–acetylene flame where there is a high proportion of nitrogen and carbon monoxide present. In fact under the conditions found in our flame, nitrogen and carbon monoxide are the two most abundant species, representing concentrations more than three orders of magnitude greater than the nascent NO concentration.[32] Therefore, based on our buffer gas observations, we would expect a significant reduction in the SPFWM sensitivity in the flame under these conditions. However, we have found the SPFWM sensitivity was only reduced by a factor of between 10 and 100 in our flame, suggesting that SPFWM is more robust than PFWM under conditions of varying refractive index.

There are three obvious reasons for the observed robustness of the SPFWM technique. The first is that the PFWM signal depends exponentially on the gain, so any reduction in gain can have a dramatic effect on the efficiency of the PFWM process, whereas, the SPFWM signal depends quadratically on the gain and so is less affected by any variation in gain. Second, the bandwidth of the seeder field must be considered. For PFWM generation, this can be quite broad[17] thus allowing phase matching to be achieved in the SPFWM process over a broad range of conditions. Finally, we have shown that SPFWM in low density media has a high tolerance to phase mismatches, this tolerance increasing with seeder field strength. So under conditions of strong seeding, appreciable gain may still be achieved. In certain cases the SPFWM gain may also be increased by the introduction of

an appropriate buffer gas into the high pressure PFWM seeder cell to appropriately shift the phase matching point.

E. Unique characteristics of SPFWM

As SPFWM is a nondegenerate near-resonance FWM technique, it has a number of unique characteristics such the ability to operate with high pump powers which act to increase the sensitivity of the technique without loss of signal due to saturation. The collinear propagation of the signal with the pump beam makes alignment of detectors quite simple, after which the pump can be simply filtered out. Furthermore, the SPFWM arrangement could allow post-generation FWM signal amplifiers to be used to increase the signal to noise ratio.

We have also found the direct absorption term of Eq. (9) is quite small due to the collinear phase matching requirement which generally finds the optimum phase matching point occurring at the periphery of the absorption profile.[20,33] Thus we readily observe a strong uv PFWM signal from the seeder cell, even when the medium is optically thick. This property is in direct contrast to DFWM which can suffer from significant signal reabsorption often limiting the sensitivity of the technique.[34] Consequently, it should be possible to provide selective molecular filtering of the signal in order to reduce any incoherent resonant background emission noise, thus increasing the signal to noise ratio. This may be especially useful for reducing the background noise in the flame spectrum of Fig. 8.

With SPFWM, the intermediate resonance acts to increase the FWM gain to such a degree that we are able to record a two-photon resonant spectrum with a sensitivity close to that achievable with single photon resonant DFWM.[1,35] This suggests that SPFWM detection of the $C\ ^2\Pi(v'=0)\leftarrow X\ ^2\Pi(v''=0)$ two-photon transition, is capable of providing spectral information with molecular concentrations far lower than many alternative two-photon resonant techniques.[30,31,36–39] Of course this requires the development of a suitable spectral model.

Finally, we emphasize that our experiments were conducted with a comparatively large bandwidth, multimode laser. The transverse spatial mode quality was poor in comparison to a single mode Gaussian beam. The theory presented is only a single mode plane-wave theory and yet it shows excellent agreement with our experimental observations. The observed gain increase between seeded and non-seeded PFWM suggests a detection sensitivity increase of over 4 orders of magnitude in molecular density. This number very closely agrees with changes in detection threshold estimates given by the theory. One would usually suspect that single mode operation would help to further improve the performance of the system, as is generally the case with FWM. However, as the effects of foreign species as well as chromatic aberration of the recollimating lens can act to compromise the phase matching within the SPFWM medium, it is possible that the poor beam quality may act to partially compensate for any phase mismatch by providing a ensemble of possible phase matching conditions. This hypothesis has yet to be tested.

V. CONCLUSION

We have shown SPFWM to be a sensitive and robust nonlinear technique useful for the detection of trace quantities of nitric oxide. Our initial investigations of NO have indicated the ability to detect samples with partial pressures below 1 μbar, with an estimated detection limit of 10^{12} molecules per cm^3, using the experimental configuration we have presented. This detection sensitivity represents a gain of over 4 orders of magnitude when compared to PFWM alone. Furthermore, we have demonstrated the ability to detect nascent NO concentrations of the order of 100 ppm in an air–acetylene flame using SPFWM. This represents operation under extreme conditions where the presence of high concentrations of molecular nitrogen and carbon monoxide have been demonstrated to adversely affect the phase matching conditions. However, we find that the SPFWM gain is still significant under these conditions, with an estimated reduction in gain of between 1 and 2 orders of magnitude when compared to the cell data, illustrating the high tolerance of SPFWM to phase mismatches in low density media.

A strong ac Stark shift in the two-photon resonance, caused by the generation of strong PFWM fields, was found in the high density seeder cell. This acts to limit the SPFWM gain in the present experiment, by reducing seeder field strength on resonance. We have also observed the seeder cell operating in the two-photon cancellation regime which also limits the ir seeder field generation. These limitations may be overcome by modifying the focal conditions within the seeder cell so that weaker fields are generated over an increased focal area such that the net effect is to increase the overall seeder intensity, thus increasing the SPFWM gain. We have also found that by increasing the seeder cell NO pressure from 300 mbar to 400 mbar, we could obtain more than an order of magnitude increase in SPFWM sensitivity. As higher pressure cells operate with considerable spectral broadening due to the increased gain, such broadening may also compensate for the observed ac Stark shift, further increasing the SPFWM gain.

A simple theoretical model of SPFWM has been developed which shows excellent agreement with the experimental data, suggesting that SPFWM may be useful for certain quantitative applications, especially when operating in the small signal regime. The model is also useful for understanding how SPFWM behaves under the highly variable conditions expected in molecular FWM processes and indicates that any molecular SPFWM spectrum must also be interpreted in terms of phase matching conditions determined by the linear susceptibility of the intermediate state. A full spectral model of SPFWM operation has not been attempted at this time. Such a model must include laser bandwidth and Doppler broadening effects as well as molecule specific information in order to determine the appropriate phase matching condition and necessary third order susceptibilities.

A major benefit of SPFWM is its simple single beam geometry. In contrast, other well known nonlinear optical techniques, such as DFWM and coherent anti-Stokes Raman scattering, require complex multiple beam geometries. The generation of a coherent signal beam at a wavelength significantly different from that of the pump beam, but which trav-

els collinearly, eliminates scattering interference and greatly simplifies system alignment and signal retrieval. We have demonstrated that the technique has a sensitivity approaching that of DFWM, even under challenging combustion conditions and, as it is a near resonant technique, it does not suffer from strong signal reabsorption as the signal is generated sufficiently far off-resonance. The unique characteristics of the technique also offer other possibilities such as FWM amplification and selective molecular filtering of the signal both of which could increase the signal to noise ratio before detection. Therefore, considering its sensitivity, simplicity and robustness, we believe SPFWM may have great potential for the remote sensing of environmentally significant atoms and molecules in hostile environments.

[1] R. L. Farrow and D. J. Rakestraw, Science **257**, 1894 (1992).
[2] S. Williams, R. Zare, and L. Rahn, J. Chem. Phys. **101**, 1093 (1994).
[3] M. A. Buntine, D. W. Chandler, and C. C. Hayden, J. Chem. Phys. **97**, 707 (1992).
[4] G. Hall and B. Whitaker, J. Chem. Soc. Faraday Trans. **90**, 1 (1994).
[5] P. H. Paul, R. L. Farrow, and P. M. Danehy, J. Opt. Soc. Am. B **12**, 384 (1995).
[6] P. M. Danehy, E. J. Friedman-Hill, R. P. Lucht, and R. L. Farrow, Appl. Phys. B: Photophys. Laser Chem. **57**, 243 (1993).
[7] E. F. McCormack, S. T. Pratt, P. M. Dehmer, and J. L. Dehmer, Chem. Phys. Lett. **211**, 147 (1993).
[8] J. Geng, T. Kobayashi, and M. Takami, Chem. Phys. Lett. **266**, 290 (1997).
[9] P. M. Danehy, P. H. Paul, and R. L. Farrow, J. Opt. Soc. Am. B **12**, 1564 (1995).
[10] R. P. Lucht, R. L. Farrow, and D. J. Rakestraw, J. Opt. Soc. Am. B **10**, 1508 (1993).
[11] E. J. Friedman-Hill, L. A. Rahn, and R. L. Farrow, J. Chem. Phys. **100**, 4065 (1994).
[12] J. Ishii, T. Matsui, K. Tsukiyama, and K. Uehara, Chem. Phys. Lett. **220**, 29 (1994).
[13] N. Bloembergen, *Nonlinear Optics* (Benjamin, New York, 1965).
[14] C. R. Vidal, *Four-wave frequency mixing in gases*, in *Tunable Lasers*, edited by L. Mollenauer and J. White (Springer, Berlin, 1987), pp. 57–113.
[15] W. Hartig, Appl. Phys. **15**, 427 (1978).
[16] J. Heinrich, K. Hollenberg, and W. Behmenburg, Appl. Phys. B: Photophys. Laser Chem. **33**, 225 (1984).
[17] R. W. Boyd, M. S. Malcuit, D. J. Gauthier, and K. Rzażewski, Phys. Rev. A **35**, 1648 (1987).
[18] M. S. Malcuit, D. J. Gauthier, and R. W. Boyd, Phys. Rev. Lett. **55**, 1086 (1985).
[19] M. J. Fernée, P. F. Barker, A. E. W. Knight, and H. Rubinsztein-Dunlop, Phys. Rev. A (in press).
[20] U. Czarnetzki and H. F. Döbele, Phys. Rev. A **44**, 7530 (1991).
[21] J. Ishii, Y. Ogi, Y. Tanaka, and K. Tsukiyama, Opt. Commun. **132**, 316 (1996).
[22] G. S. Agarwal, Phys. Rev. Lett. **57**, 827 (1986).
[23] S. E. Harris, J. E. Field, and A. Imamoğlu, Phys. Rev. Lett. **64**, 1107 (1990).
[24] J. C. Petch, C. H. Keitel, P. L. Knight, and J. P. Marangos, Phys. Rev. A **53**, 543 (1996).
[25] G. Z. Zhang, K. Hakuta, and B. P. Stoicheff, Phys. Rev. Lett. **71**, 3099 (1993).
[26] M. Jain, G. Y. Yin, J. E. Field, and S. E. Harris, Opt. Lett. **18**, 998 (1993).
[27] M. J. Fernée, P. F. Barker, A. E. W. Knight, and H. Rubinsztein-Dunlop, Phys. Rev. Lett. **79**, 2046 (1997).
[28] M. J. Fernée, P. F. Barker, H. Rubinsztein-Dunlop, and A. E. W. Knight (unpublished).
[29] R. Loudon, *The Quantum Theory of Light*, 2nd ed. (Clarendon, Oxford, 1983).
[30] P. A. Freedman, Can. J. Phys. **55**, 1387 (1977).
[31] J. S. Hayden and G. J. Diebold, J. Chem. Phys. **77**, 4767 (1982).
[32] C. Alkemade, T. Hollander, W. Snellman, and P. Zeegers, *Metal Vapours in Flames* (Pergamon, Oxford, 1982), Ch. IV.
[33] R. K. Wunderlich, W. R. Garrett, R. C. Hart, M. A. Moore, and M. G. Payne, Phys. Rev. A **41**, 6345 (1990).
[34] P. Ljungberg and O. Axner, Appl. Opt. **34**, 527 (1995).
[35] E. Konz, V. Fabelinsky, G. Marowsky, and H. Rubahn, Chem. Phys. Lett. **247**, 522 (1995).
[36] M. Asscher and Y. Haas, Chem. Phys. Lett. **59**, 231 (1978).
[37] W. M. Jackson and C. S. Lin, Int. J. Chem. Kinet. **10**, 945 (1978).
[38] N. Georgiev, U. Westblom, and M. Alden, Opt. Commun. **94**, 99 (1992).
[39] J. A. Gray and R. Trebino, Chem. Phys. Lett. **216**, 519 (1993).